phys. stat. sol. (b) **245**, No. 12, 2800–2807 (2008) / **DOI** 10.1002/pssb.200844142

physica status solidi b
www.pss-b.com
basic solid state physics

Structural, electronic and optical properties of spinel $MgAl_2O_4$ oxide

S. M. Hosseini*

Department of Physics (Materials and Electroceramics Laboratory), Ferdowsi University of Mashhad, Iran

Received 6 April 2008, revised 13 May 2008, accepted 25 June 2008
Published online 8 August 2008

PACS 71.15.Mb, 71.20.–b, 78.20.Ci

* e-mail sma_hosseini@yahoo.com, Phone: +98 511 8435723, Fax: +98 511 8796416

The structure, band structure, total density of states, dielectric function, reflectivity, refractive index and loss function have been calculated for spinel $MgAl_2O_4$ oxide using density functional theory. The full-potential linearized augmented plane wave method was used with the generalized gradient approximation. Calculations of the optical spectra have been performed for the energy range 0–40 eV. It is shown that the material is transparent at visible wavelengths and the dispersion curve of the refractive index is fairly flat in the long-wavelength region and rises rapidly towards shorter wavelengths. The refractive index is 1.774 at 800 nm near the visible region.

1 Introduction The spinel structure (sometimes called garnet structure) is named after the mineral *spinel* ($MgAl_2O_4$); the general composition is AB_2O_4. The spinel structure has a close-packed face-centred cubic structure of space group Fd3m (number 227), with eight $MgAl_2O_4$ units per cubic cell [1]. Three degrees of freedom associated with the detailed atomic arrangements of spinels are: (i) the lattice parameter, a; (ii) the anion parameter, u; and (iii) the cation inversion parameter. The cations (usually metals) occupy 1/8 of the tetrahedral sites and 1/2 of the octahedral sites and there are 32 oxygen ions in the unit cell. The anion sublattice is arranged in a pseudo-cubic close packed (ccp) spatial arrangement. Some spinels possess almost ideal ccp anion sublattices. The description of the atomic positions in spinel is dependent on the choice of setting for the origin in the Fd3m space group. Two different equipoints with point symmetries $\bar{4}3m$ and $\bar{3}m$ are possible choices for the unit cell origin. Moreover, the origin can be assigned to either a vacant site or an occupied lattice site. The coordinates of the anions at equipoints 32e are not special: they vary according to a single parameter, u for a perfect ccp anion arrangement, $u_{\text{ideal}}^{\bar{4}3m} = 3/8$ (0.375) and $u_{\text{ideal}}^{\bar{3}m} = 1/4$ (0.250) for origins at $\bar{4}3m$ and $\bar{3}m$, respectively [2].

The spinel structure is very flexible with respect to the cations it can incorporate; there are over 100 known compounds. In particular, the A and B cations can mix. In other words, the composition with respect to one unit cell can be $(A_8)(B_{16})O_{32}$ or $A_8(B_8A_8)O_{32} = A(AB)O_4$ in regular chemical notation, or $(A_{8/3}B_{16/3})(A_{16/3}B_{32/3})O_{32}$, and so on, with the atoms in the parentheses occupying the respective site at random. Two types of spinels can be distinguished: normal and inverse spinels. In the normal spinel, all Al^{3+} ions are in octahedral coordination with local symmetry D_{3d}, and all Mg^{2+} ions are in tetrahedral coordination with point group symmetry T_d. Thus the general formula may be written as $(Mg)[Al_2]O_4$ or $(Mg_8)[Al_{16}]O_{32}$ for the cubic cell, where ( ) and [ ] denote tetrahedral and octahedral sites, respectively. The Mg–O and Al–O bond lengths in the normal spinel are 1.967 Å and 1.855 Å, respectively [3]. $MgAl_2O_4$ single crystals are widely used for bulk acoustic wave and microwave devices and fast IC epitaxial substrates. It is also found that $MgAl_2O_4$ is a good substrate for III–V nitride devices [4].

The spinel oxides comprise an important class of ceramic compounds with a variety of interesting electrical, magnetic and optical properties. The magnesium spinel $MgAl_2O_4$ has a combination of desirable properties of high melting point (1250 °C), high strength, resistance to chemical attack and low electrical losses [5]. These special properties mean that a magnesium spinel has many important applications. It has been reported that $MgAl_2O_4$ thin films show interesting characteristics in terms of their use in humidity measurement devices [6, 7].

A few computational approaches have also been made to investigate the structure and the electronic structure of spinel $MgAl_2O_4$ such as lattice constants, internal oxygen position and band gap. Wei and Zhang [8] have used a first-principles band-structure method. They have systematically studied the cation distribution in closed-shell $A^{II}B_2^{III}O_4$ and $A^{IV}B_2^{II}O_4$ spinels where the group II atoms are Mg, Zn and Cd, the group III atoms are Al, Ga and In and the group IV atoms are Si, Ge and Sn. The total energies, the structural parameters and the band gaps of these compounds in both normal and inverse spinel structures have been calculated. Mo and Ching [3] have studied the electronic structure of normal, inverse and partially inverse spinels in the $MgAl_2O_4$ system by means of first-principles calculations. Catti et al. [9] have calculated the ground-state crystal energies of cubic $MgAl_2O_4$ (spinel), MgO (periclase) and rhombohedral α-Al_2O_3 (corundum) at different volumes, relaxing the corresponding structure, by the all-electron periodic Hartree–Fock method (CRYSTAL program). Khenata et al. [10] have studied theoretically the structural, elastic and electronic properties of spinel $MgAl_2O_4$ and $ZnAl_2O_4$ oxides using the full-potential linear augmented plane wave (FP-LAPW) method as implemented in the WIEN97 code. In this approach the local density approximation (LDA) was used for the exchange-correlation (XC) potential. Sampath et al. [11] studied the electronic structure of zinc aluminate ($ZnAl_2O_4$) and zinc gallate ($ZnGa_2O_4$) by the self-consistent tight-binding linearized muffin-tin orbital method with the atomic sphere approximation.

However, to our knowledge, only a few theoretical and experimental articles have been published on the optical properties of spinel $MgAl_2O_4$ oxide. Xu and Ching [12] have studied the electronic structure, the charge density distribution and the optical absorption spectra of MgO, α-Al_2O_3 and $MgAl_2O_4$ crystal by the orthogonalized linear combination of atomic orbitals method. Thibaudeau and Gervais [13] have performed *ab initio* calculations of infrared and Raman phonon modes in the normal cubic $MgAl_2O_4$ spinel at the first Brillouin zone centre using density functional theory (DFT) with plane-wave basis and norm-conserving pseudopotentials. Bortz et al. [14] have studied the room temperature optical reflectivity of MgO, $MgAl_2O_4$ and α-Al_2O_3 from 5 eV to 40 eV using a novel spectrophotometer with a laser plasma light source.

In this paper the structure, band structure, total density of states and optical properties such as the dielectric function, reflectivity, refractive index and loss function of $MgAl_2O_4$ are calculated within the frame of the random phase approximation using DFT.

2 Structure The structure of spinel is based on the structure of diamond. The positions of the A ions are nearly identical to the positions occupied by carbon atoms in the diamond structure. This could explain the relatively high hardness and high density typical of this group. The arrangements of the other ions in the structure conform to the symmetry of the diamond structure. However, they disrupt the cleavage as there are no cleavage directions in any member of this group.

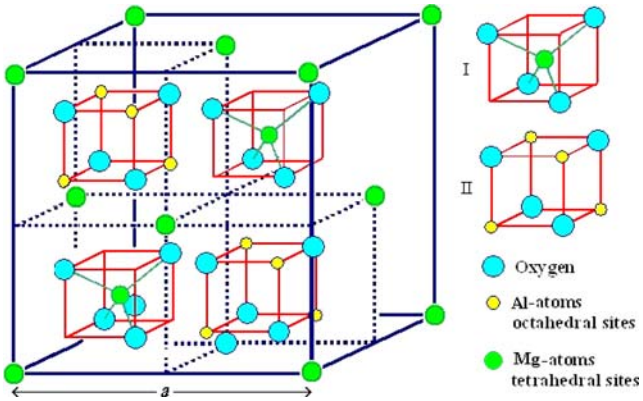

Figure 1 (online colour at: www.pss-b.com) Primitive tetrahedral unit cell of spinel $MgAl_2O_4$. The cubic cell consists of eight constants of type I and II.

The primitive tetrahedral unit cell of spinel $MgAl_2O_4$ is illustrated in Fig. 1. Inside the cell, with eight formula units per cubic cell, each magnesium ion is tetrahedrally coordinated to four oxygen atoms while each aluminium atom is surrounded by six octahedrally distributed atoms. The structure consists of eight octants of type I and type II as shown in Fig. 1. The type I octants contain magnesium ions in tetrahedral coordination and the type II octants contain aluminium ions in octahedral coordination. There are 96 interstices between the anions in the cubic unit cell; however, in AB_2O_4 compounds, only 24 are occupied by cations. Of the 64 tetrahedral interstices that exist between the anions, 8 are occupied by cations. The remaining 16 cations occupy half of the 32 octahedral interstices. The tetrahedrally coordinated cations form a diamond cubic sublattice with a repeat unit equal to the lattice parameter. The periodicity associated with the sublattice of octahedrally coordinated cations also is equal to the spinel lattice parameter (a).

3 Method of calculation The calculations and relaxation of the ionic positions were carried out with a self-consistent scheme by solving the Kohn–Sham equations using a FP-LAPW method in the framework of DFT along with the generalized gradient approximation (GGA) [15, 16] using Wien2k codes [17]. Since the calculation of dielectric tensor requires a dense mesh of eigenvalues and the corresponding eigenvectors, the calculation of complex dielectric tensor was performed with a fine k-mesh using 1000 k-point in the irreducible wedge of first Brillouin zone. The values of other parameters are $Rk_{max} = 7$ (R is the smallest muffin-tin radius and k_{max} is the cut-off for the plane wave) for the convergence parameter, $G_{max} = 14$ (magnitude of largest vector in charge density Fourier expansion or the plane wave cut-off), and $R_{MT}(Mg) = 1.8$ au, $R_{MT}(Al) = 1.9$ au and $R_{MT}(O) = 1.75$ au (muffin-tin radii).

The iteration halted when the charge difference was less than 0.0001e between steps as convergence criterion. The cut-off energy, which defines the separation of valence and core states, was chosen as −6 Ry.

3.1 Structure optimization

3.1.1 Lattice parameters From the literature, we know that the bulk elastic properties of a material determine how much it will compress under a given amount of external pressure. The ratio of the change in pressure to the fractional volume compression is called the bulk modulus (B) of the material and can be written as

$$B = -V\frac{\partial P}{\partial V}. \tag{1}$$

In terms of energy, the bulk modulus is also defined by the equation of state (EOS) and evaluated at the minimum as

$$B = V\frac{\partial^2 E}{\partial V^2}. \tag{2}$$

The position of the minimum of the EOS defines the equilibrium lattice parameter and unit cell volume at zero pressure. The static lattice potential corresponding to total energy was calculated from a series of strained lattices. From such results the equilibrium volume, bulk modulus and its pressure derivative were derived. A series of total energy calculations as a function of volume can be fitted to an EOS according to Murnaghan [18]:

$$E(V) = E_0 + \frac{B_0 V}{B_0'}\left[\frac{(V_0/V)^{B_0'}}{B_0'} + 1\right] - \frac{B_0 V_0}{B_0' - 1} \tag{3}$$

where B_0 is an equilibrium bulk modulus that effectively measures the curvature of the energy versus volume curve about the relaxed volume V_0, and B_0' is the derivative of the bulk modulus.

3.1.2 Atomic relaxation Most structures have free internal structural parameters, which can either be taken from experiment or optimized using the calculated forces on the nuclei. Almost all optimization codes use what is called a quadratic approximation; they expand the energy in the form

$$E^* = E + \boldsymbol{g}^{\mathrm{T}}\boldsymbol{s} + \left(\tfrac{1}{2}\right)\boldsymbol{s}^{\mathrm{T}}\boldsymbol{H}\boldsymbol{s} \tag{4}$$

where E^* is the predicted energy for a step $\boldsymbol{s}$ from the current point, E and $\boldsymbol{g}$ are the energy and gradient (negative of the force) calculated at the current point and $\boldsymbol{H}$ is the Hessian matrix.

Different algorithms use different approaches to the Hessian matrix. The most primitive is steepest descent, which takes $\boldsymbol{H}$ as the unitary matrix so will take a step along the direction of the force [19]. For atomic relaxation of $MgAl_2O_4$, we used the reverse-communication trust region quasi-Newton method from the Port library which seems to be stable, efficient and does not depend too much on the user input as implemented in the Wien2k package.

3.1.3 Optical properties The band-to-band transition of an electron from the valence to conduction band is induced by incident light. The photon energy absorbed in the material per unit time and unit volume is equivalent to the power dissipation of electromagnetic wave per unit time and unit volume and thus is related to the imaginary part of the dielectric tensor via the equation [20]

$$\mathrm{Im}\,\varepsilon(\omega) = \frac{\pi e^2}{\varepsilon_0 m^2 \omega^2}\sum_{c,v}|\boldsymbol{e}\cdot\boldsymbol{p}_{cv}|^2\,\delta[\varepsilon_{c_k} - \varepsilon_{v_{k'}} - \hbar\omega]\,\delta_{\boldsymbol{k}\boldsymbol{k}'} \tag{5}$$

where $\boldsymbol{e}\cdot\boldsymbol{p}_{cv}$ is the matrix element for a transition from a filled valence state of wave vector $\boldsymbol{k}'$ to an empty conduction state of wave vector $\boldsymbol{k}$.

The dielectric function of an anisotropic material is a complex symmetric tensor. In the limit of linear optics, in the case of non-spin polarization, and within the independent particle approximation, random phase approximation (RPA), the imaginary part of the dielectric tensor can be computed from knowledge of the electronic band structure of a solid from the well-known relation [21]

$$\mathrm{Im}\,\varepsilon_{\alpha\beta}(\omega) = \frac{4\pi e^2}{m^2\omega^2}\sum_{c,v}\int \mathrm{d}\boldsymbol{k}\,\langle c_{\boldsymbol{k}}|\,p^{\alpha}|v_{\boldsymbol{k}}\rangle\langle v_{\boldsymbol{k}}|\,p^{\beta}|c_{\boldsymbol{k}}\rangle \times \delta(\varepsilon_{c_k} - \varepsilon_{v_k} - \omega]) \tag{6}$$

where $|v_{\boldsymbol{k}}\rangle$ and $|c_{\boldsymbol{k}}\rangle$ are electron states in the valence and the conduction bands, respectively, with wave vector $\boldsymbol{k}$. The real part of the frequency-dependent dielectric function $\varepsilon_{\alpha\beta}(\omega)$ is given by

$$\mathrm{Re}\,\varepsilon_{\alpha\beta}(\omega) = \delta_{\alpha\beta} + \frac{2}{\pi}P\int_0^{\infty}\frac{\omega'\,\mathrm{Im}\,\varepsilon_{\alpha\beta}(\omega')}{\omega'^2 - \omega^2}\,\mathrm{d}\omega', \tag{7}$$

which is named after Ralph Kronig and Hendrik Anthony Kramers, and where P is the Cauchy principal value.

The Kramers–Kronig relations allow calculation of the refractive index and other optical constant profiles from the frequency-dependent losses, which can be calculated over a large spectral range. The refractive index, $n(\omega)$, and the extinction coefficient, $k(\omega)$, are given by [22]

$$n_{\alpha\beta}(\omega) = \left\{\tfrac{1}{2}\left[\left|\varepsilon_{\alpha\beta}(\omega)\right| + \mathrm{Re}\,\varepsilon_{\alpha\beta}(\omega)\right]\right\}^{1/2} \tag{8}$$

and

$$k_{\alpha\beta}(\omega) = \left\{\tfrac{1}{2}\left[\left|\varepsilon_{\alpha\beta}(\omega)\right| - \mathrm{Re}\,\varepsilon_{\alpha\beta}(\omega)\right]\right\}^{1/2}. \tag{9}$$

At low frequency the static refractive index $n_{\alpha\beta}(0)$ can be calculated using the following expression for nonmagnetic materials:

$$n_{\alpha\beta}^2(0) = \mathrm{Re}\,\varepsilon_{\alpha\beta}(\infty) \tag{10}$$

where $\varepsilon_{\alpha\beta}(\infty)$ is the high-frequency dielectric constant. The dielectric tensor is symmetric with up to six independent components according to the symmetry of the crystal. For the spinel $MgAl_2O_4$ structure, the optical properties are isotropic, i.e. there is only one independent component (ε_{xx}).

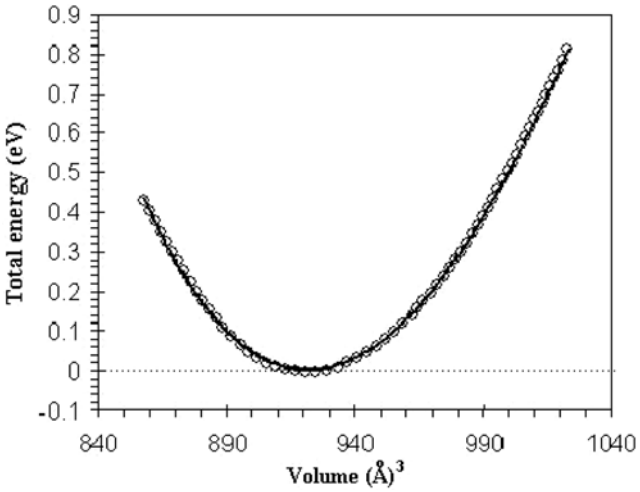

Figure 2 Calculated total energies versus volume for spinel $MgAl_2O_4$ oxide.

4 Results and discussion

4.1 Electronic structure The calculations first were carried out applying the experimental data for lattice constant $a = 8.0898$ Å [23] then, by minimizing the total energy of the crystal to the volume, the theoretical lattice constant was obtained as $a = 8.1745$ Å. Figure 2 shows the calculated total GGA energy E_{tot} as a function of crystal volume for the spinel $MgAl_2O_4$ oxide.

We minimized the energy for atomic positions and determined the equilibrium position of individual atoms. The final calculation was performed with the theoretical lattice constant and relaxed structure. The results of a full relaxation of anion positions in the Fd3m structure of $MgAl_2O_4$ are summarized in Table 1.

4.2 Electronic properties The calculated electronic band structure for the spinel $MgAl_2O_4$ oxide along the high symmetry directions is shown in Fig. 3.

The calculations were performed using GGA with the relaxed atomic positions. The overall band profiles calculated in this work are consistent with other first-principles calculation results reported previously [10, 11]. The scale of energy in all figures is in eV and the top of the valence band is set to zero (Fermi level) on the energy scale. The valence bands are separated by a 5.2 eV direct gap at Γ-point from the conduction band states. Experimentally, the optical reflectivity measurements reported the minimum band gap of $MgAl_2O_4$ to be direct at Γ with a value of 7.8 eV [14]. Our calculated band gap is smaller than the experimental values. This discrepancy mainly arises from the GGA, which is known to underestimate the energy band gap of insulators. There are two indirect band gaps in the [111] and [101] directions, along Γ–L and Γ–X, with values of 7.5 and 8.2 eV, respectively.

Figure 4 shows the calculated total density of states for the $MgAl_2O_4$ spinel structure. The lower O 2s band splits into two: a very sharp peak at −16.0 eV and a lower part 2.0 eV wide with double peaks. The sharp structures in the energy range −18.2 to −15.5 eV are mainly due to O 2s states. The upper valence band is composed mostly of O 2p states and hybridized with Mg 3s and Al 3p orbitals. The conduction band has compounds from both Mg 3s and Al 3p states.

The electron density of spinel $MgAl_2O_4$ oxide in the (100) plane for two and three dimensions is plotted in Fig. 5. This plane does not contain any magnesium ions and shows the oxygen ions (large circles) and aluminium ions (small circles) which are arranged diagonally between each other.

In Fig. 6 the electron density in the (110) plane for two and three dimensions is shown. This plane contains all three types of ions. Between two rows of magnesium ions of this plane there is an empty channel with almost no or little charge.

Table 1 Calculated and experimental crystallographic data for spinel $MgAl_2O_4$ oxide with space group Fd3m.

Wyckoff position	ionic positions (x, y, z)			
	perfect ccp anion arrangement $u_{ideal}^{\bar{3}m}$ [2]	experimental [23] (neutron powder diffraction)	theoretical [13] (LDA)	theoretical (GGA) (this work)
Mg (8a)	(1/8, 1/8, 1/8)	(1/8, 1/8, 1/8)	(1/8, 1/8, 1/8)	(1/8, 1/8, 1/8)
Al (16d)	(1/2, 1/2, 1/2)	(1/2, 1/2, 1/2)	(1/2, 1/2, 1/2)	(1/2, 1/2, 1/2)
O (32e)	(1/4, 1/4, 1/4)	(0.261714, 0.261714, 0.261714)	(0.2735, 0.2735, 0.2735)	(0.2632, 0.2632, 0.2632)
		experimental	theoretical	this work
lattice constant, a (Å)		8.08360 [23]	8.0832 [8], 8.027 [11], 7.905 [13]	8.1074
bulk modulus, B (GPa)		196 [24]	213 [9], 220 [11], 199 [13]	188.4
derivative of the bulk modulus, B'		4.89 [24]	5.40 [9], 2.95 [11], 3.66 [13]	4.4503
bond lengths (Å):				
Mg–O		–	1.96 [8]	1.9569
Al–O		–	1.82 [8]	1.9416

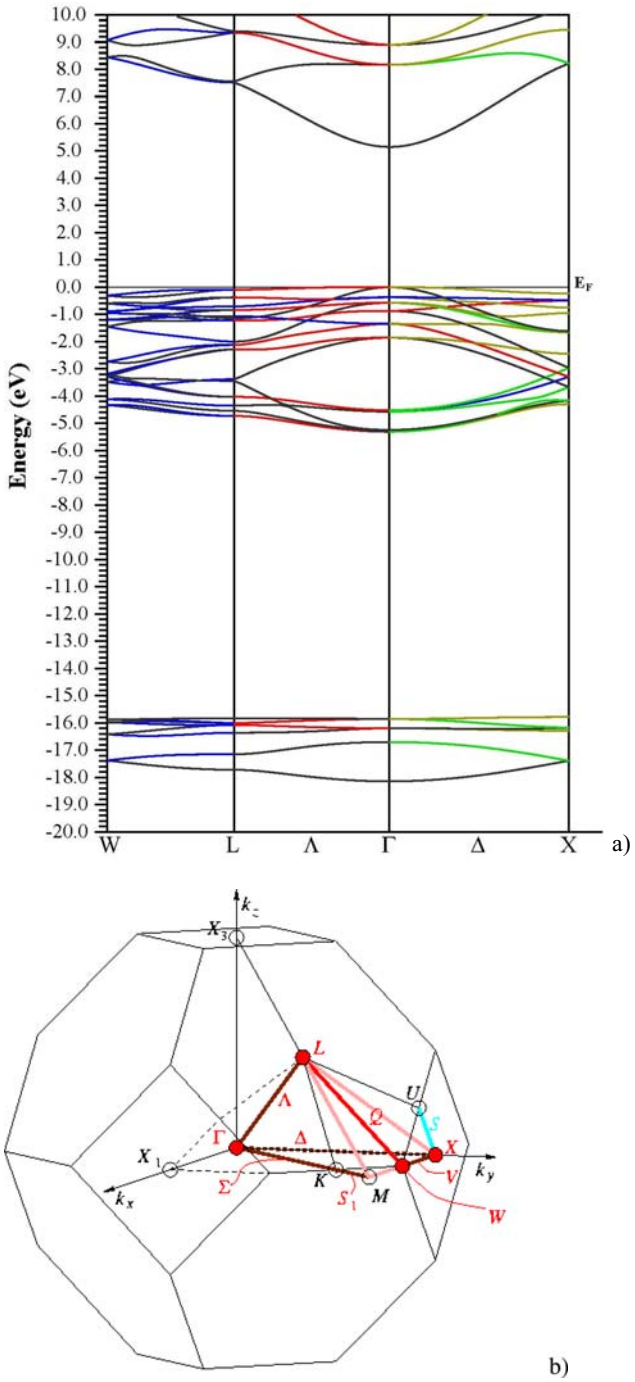

Figure 3 (online colour at: www.pss-b.com) a) Band structure and b) the first Brillouin zone of spinel $MgAl_2O_4$ structure.

4.3 Optical properties

The real and imaginary parts of the frequency-dependent dielectric function for the spinel $MgAl_2O_4$ structure are shown in Fig. 7. The static dielectric permittivity tensor, $\varepsilon_{\alpha\beta}(0)$, of a nonpolar material contains electronic (high-frequency) and ionic contributions. The high-frequency dielectric constant, $\varepsilon(\infty)$, of spinel $MgAl_2O_3$ oxide is presented in Table 3. The calculated Im $\varepsilon(\omega)$ shows the first peak at about $E_0 = 6.27$ eV;

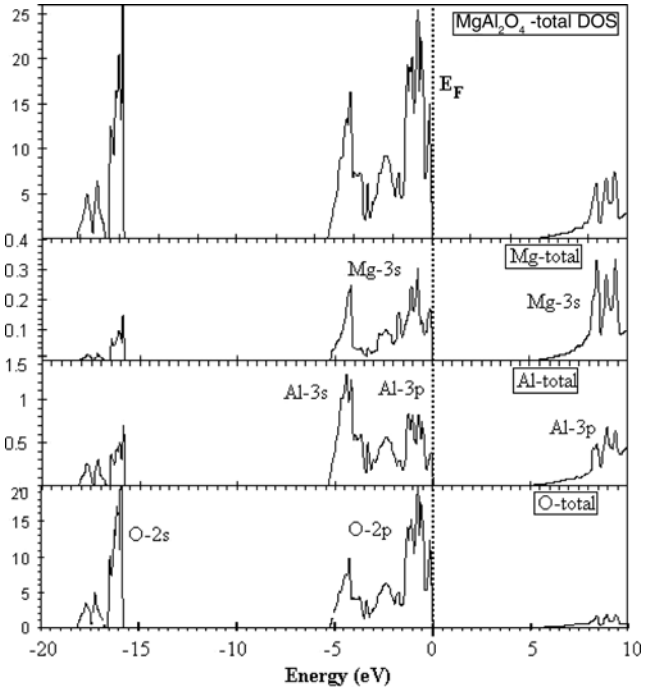

Figure 4 Total density of states (DOS) of spinel $MgAl_2O_4$ structure and total Mg, Al and O atoms.

this is due to the fundamental gap. This peak is related to the interband transition from the valence to the conduction band states along Γ–Γ direction. For simplification of analysis of the other optical transition spectra, the labels E_0, E_1 and E_2 have been used. The subscript 0 in E refers to transition along [000] and 1 for transitions at points in [111] direction and 2 for transitions in the [100] direction of $\boldsymbol{k}$ space. These notations are used based on those of Ref. [25] to describe the reflectivity spectra of semiconductors of wurtzite and zinc blend structures. For the spinel structure with space group Fd3m (number 227), the [111] direction is along Γ–L and [100] is from Γ–X.

The most important contribution to the peaks E_1 and E_2 arises from the transitions from the uppermost valence band to the first conduction band. The major contributions to the intensity of these peaks are throughout the large volume of the Brillouin zone. The positions of five peaks in the imaginary part of the dielectric function calculated in this work are summarized in Table 2.

Table 2 Peak values of the imaginary part for spinel $MgAl_2O_4$ oxide for transition from the uppermost valence to conduction band.

peak	energy (eV) (this work)	experimental
E_0 ($\Gamma \rightarrow \Gamma$)	6.27	7.8 [14]
E_0' ($\Gamma \rightarrow \Gamma$)	9.42	11.0 [14]
E_1 ($\Gamma \rightarrow$ L)	7.44	
E_1' ($\Gamma \rightarrow$ L)	10.19	
E_2 ($\Gamma \rightarrow$ X)	8.61	

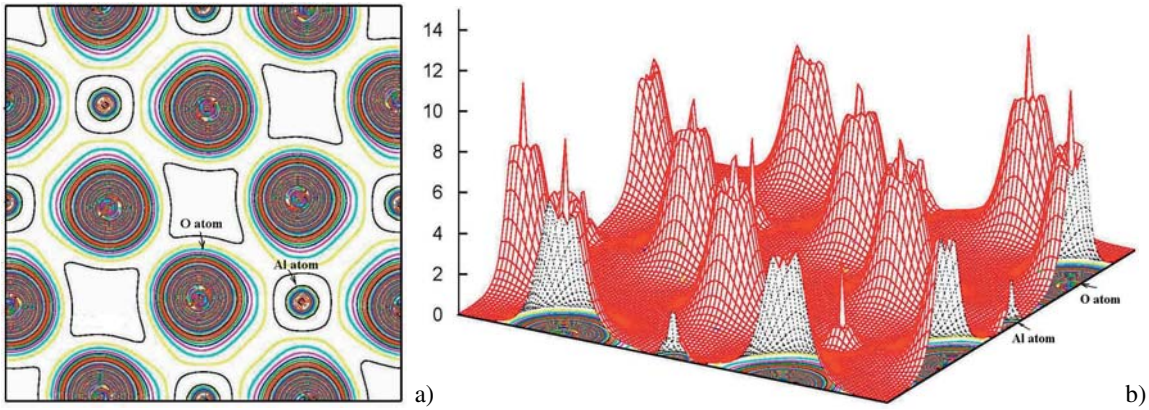

Figure 5 (online colour at: www.pss-b.com) Electron densities of spinel $MgAl_2O_4$ oxide in the (100) plane in a) two and b) three dimensions.

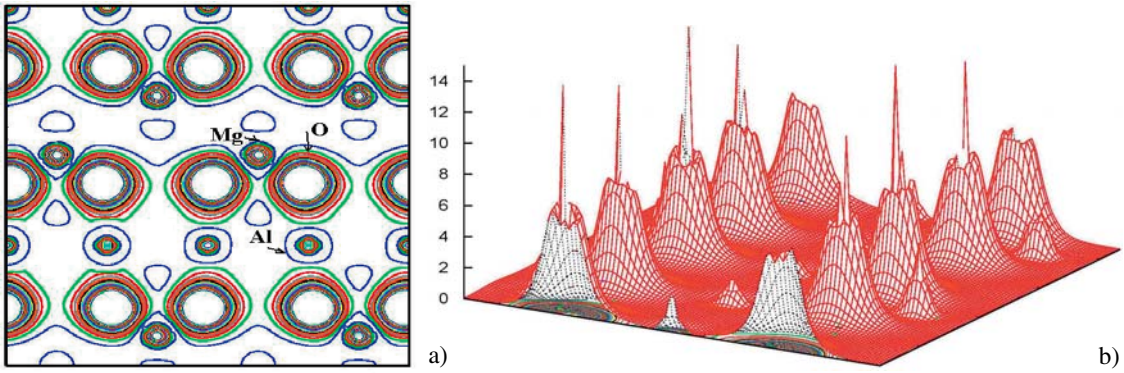

Figure 6 (online colour at: www.pss-b.com) Electron densities of spinel $MgAl_2O_4$ oxide in the (110) plane in a) two and b) three dimensions.

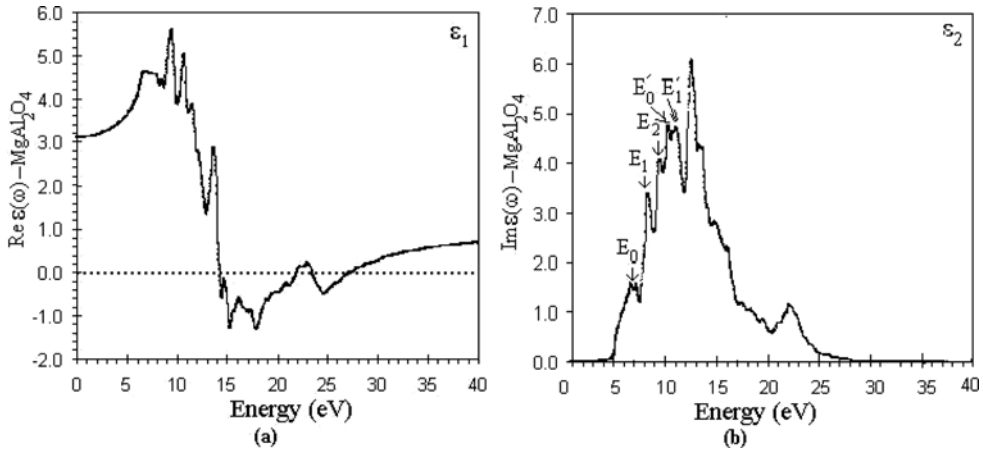

Figure 7 Calculated a) real and b) imaginary parts of the dielectric function for spinel $MgAl_2O_4$ oxide.

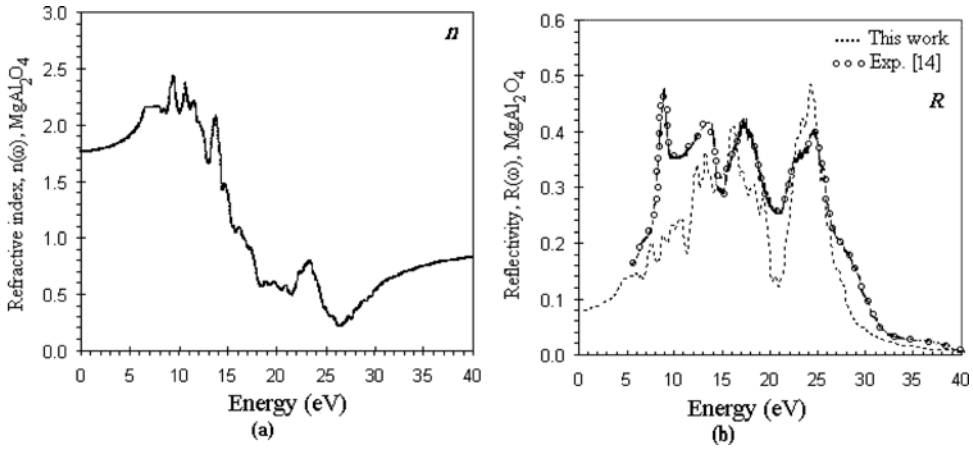

Figure 8 a) Refractive index and b) reflectivity for spinel $MgAl_2O_4$ oxide.

In Fig. 8 the refractive index, $n(\omega)$, and the reflectivity, $R(\omega)$, are shown for spinel $MgAl_2O_4$ structure. The material is transparent in the visible and the excitonic transition associated with the fundamental absorption edge increases in the series from 6.27 eV to 10.19 eV. At phonon energies above 24.5 eV the reflectivity magnitudes begin to decrease and the interband transitions are exhausted by 40 eV. The experimental spectrum of reflectivity of $MgAl_2O_4$ from 5 to 40 eV using a novel spectrophotometer with a laser plasma light source is also plotted in Fig. 8 [14].

In order to obtain an accurate value of static dielectric constant, we should add to the electronic part the optical phonon contribution. However, in this calculation we did not include such a contribution and the values of high frequency dielectric constant have been evaluated at nearly zero value of energy. The refractive index is then obtained from Eq. (10) as $n(0) \approx 1.763$ which is close to the experimental value of 1.71 [26]. The static refractive index is summarized in Table 3.

4.3.1 Dispersion of the refractive index The dispersion curve of the refractive index is shown in Fig. 9. The curve is fairly flat in the long-wavelength region and rises rapidly towards shorter wavelengths, showing the typical shape of a dispersion curve near an electronic interband transition.

The strong increase in the refractive index is associated with the fundamental band gap absorption. The refractive index is 1.774 at 800 nm near the visible region; the wavelengths of visible light are shaded.

Table 3 Refractive indices and high-frequency dielectric constants for spinel $MgAl_2O_4$ oxide.

method	$n(0)$	$\varepsilon(\infty)$
experimental:		
bulk	1.712–1.762 [26]	2.89 [28]
thin film	1.69–1.73 [27]	
theoretical	1.7320 [13]	3.00 [13]
theoretical (this work)	1.763	3.112

4.3.2 Electron energy loss spectroscopy Plasmon losses correspond to a collective oscillation of the valence electrons and their energy is related to the density of valence electrons. In the case of interband transitions, which consist mostly of plasmon excitations, the scattering probability for volume losses is directly connected to the energy loss function. One can then calculate the electron energy loss spectrum from the following relations [21]:

$$\varepsilon_{\alpha\beta}(\omega) = \varepsilon_1 + \mathrm{i}\varepsilon_2$$

and

$$L_{\alpha\beta}(\omega) = \mathrm{Im}\left[\frac{-1}{\omega_{\alpha\beta}(\omega)}\right] = \frac{\varepsilon_2}{\varepsilon_1^2 + \varepsilon_2^2}. \qquad (11)$$

In Fig. 10 the energy loss function is plotted for spinel $MgAl_2O_4$ oxide. There are other peaks and features in this spectrum, in addition to the plasmon peak, associated with interband transitions. The plasmon peak is usually the most intense feature in the spectrum and this is at an energy where Re $\varepsilon(\omega)$ goes to zero, after the zero-loss peak; the

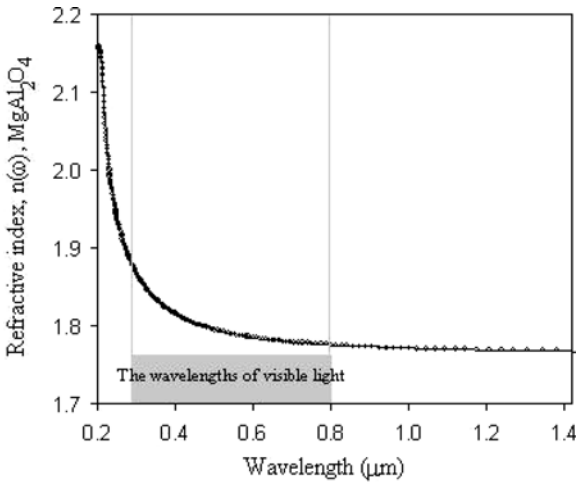

Figure 9 Wavelength dispersion curve of the refractive index for spinel $MgAl_2O_4$ oxide.

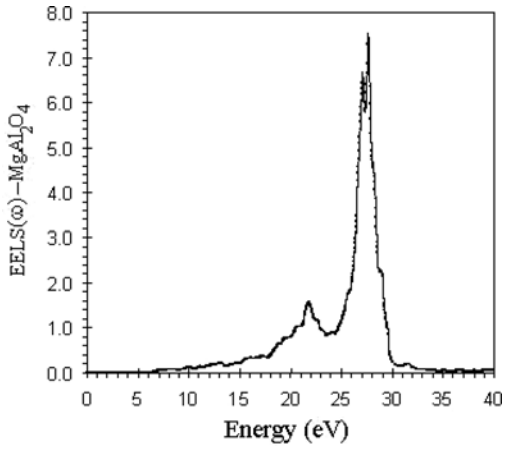

Figure 10 Loss function for the spinel $MgAl_2O_4$ oxide.

zero-loss peak is absent in Fig. 10. These spectra are broadened by only 0.1 eV and therefore will not look exactly like the experimental spectra.

The energy of the maximum peak of Im $[-\varepsilon^{-1}(\omega)]$ at 27.66 eV is assigned to the energy of volume Plasmon $\hbar\omega_p$. At this energy the real part of the dielectric function goes through zero. The various calculated energy loss values obtained in this study correspond to different transitions. The spectra of electron energy loss consist of a series of low-lying peaks between 0 eV and 25 eV associated with interband transitions. Some spectra also show a broad weak peak and we observe several peaks and a rather broad spectrum.

5 Conclusions In this work, the structural, electronic and optical properties of spinel $MgAl_2O_4$ oxide have been calculated using DFT. We calculated and analyzed the band structure and the optical constant spectra as function of the incident photon energy. The calculated results show a 5.2 eV direct band gap along the Γ–Γ direction for this structure.

The material is transparent at visible wavelengths and the excitonic transition associated with the fundamental absorption edge increases in the series from 6.27 eV to 10.19 eV. The dispersion curve of refractive index is fairly flat in the long-wavelength region and rises rapidly towards shorter wavelengths, showing the typical shape of a dispersion curve near an electronic interband transition. The refractive index value is 1.774 nm at 800 nm near the visible region.

References

[1] R. J. Hill, J. R. Graig, and G. V. Gibbs, Phys. Chem. Miner. **4**, 317 (1979).
[2] K. E. Sickafus, J. M. Wills, and N. W. Grimes, J. Am. Ceram. Soc. **82**, 3279 (1999).
[3] Shang-Di Mo and W. Y. Ching, Phys. Rev. B **54**, 16555 (1996).
[4] MII Corporation, Crystals substrates, http://www.mtixtl.com/index.asp?PageAction=VIEWCATS&Category=234
[5] C. Baudín, R. Martínez, and P. Pena, J. Am. Ceram. Soc. **78**, 1857 (1995).
[6] G. Gusmano, G. Montesperelli, E. Traversa, and G. Mattogno, J. Am. Ceram. Soc. **76**, 743 (1993).
[7] G. Gusmano, G. Montesperelli, P. Nunziante, and E. Traversa, Electrochim. Acta **38**, 2617 (1993).
[8] Su-Huai Wei and S. B. Zhang, Phys. Rev. B **63**, 045112 (2001).
[9] M. Catti, G. Valerio, R. Dovesi, and M. Causà, Phys. Rev. B **49**, 14179 (1994).
[10] R. Khenata, M. Sahnoun, H. Baltache, M. Rérat, A. H. Reshak, Y. Al-Douri, and B. Bouhafs, Phys. Lett. A **344**, 271 (2005).
[11] S. K. Sampath, D. G. Kanhere, and R. Pandey, J. Phys.: Condens. Matter **11**, 3635 (1999).
[12] Yong-Nian Xu and W. Y. Ching, Phys. Rev. B **43**, 4461 (1991).
[13] P. Thibaudeau and F. Gervais, J. Phys.: Condens. Matter **14**, 3543 (2002).
[14] M. L. Bortz, R. H. French, D. J. Jones, R. V. Kasowski, and F. S. Ohuchi, Phys. Scr. **41**, 537 (1990).
[15] J. P. Perdew, J. A. Chevary, S. H. Vosko, K. A. Jackson, M. R. Pederson, D. J. Singh, and C. Fiolhais, Phys. Rev. B **46**, 6671 (1992).
[16] M. Peterson, F. Wanger, L. Hufnagel, M. Scheffler, P. Blaha, and K. Schwarz, Comput. Phys. Commun. **126**, 294 (2000).
[17] P. Blaha, K. Schwarz, G. Madsen, D. Kvasnicka, and J. Luitz, Institute of Materials Chemistry, TU Vienna, http://www.wien2k.at/.
[18] F. D. Murnaghan, Proc. Natl Acad. Sci. **30**, 244 (1944).
[19] L. D. Marks, www.wien2k.at/reg_user/textbooks/Optimization-Notes.pdf (2004).
[20] V. Grasso, Electronic Structure and Electronic Transitions in Layered Materials (Springer, 1986).
[21] C. Ambrosch-Draxl and J. O. Sofo, Comput. Phys. Commun. **175**, 1 (2006).
[22] F. Wooten, Optical Properties of Solids (Academic Press, New York, 1972).
[23] R. C. Peterson, G. A. Lager, and R. L. Hitterman, Am. Mineralogist **76**, 1455 (1991).
[24] M. B. Kruger, J. H. Nguyen, W. Caldwell, and R. Jeanloz, Phys. Rev. B **56**, 1 (1997).
[25] M. Cardona and G. Harbeke, Phys. Rev. **137**, A1468 (1965).
[26] GEMSELECT, http://www.gemselect.com/gem-info/spinel/spinel-info.php.
[27] J. H. Boo, S. B. Lee, S. J. Ku, W. Koh, C. Kim, K. S. Yu, and Y. Kim, Appl. Surf. Sci. **169/170**, 581 (2001).
[28] N. N. Boguslavska, E. F. Venger, N. M. Vernidub, Yu. A. Pasechnik, and K. V. Shportko, Semicond. Phys. Quantum Electron. Optoelectron. **5**, 95 (2002).